Catalytic Oxidation of NO over MnOx–CeO2 and MnOx–TiO2 Catalysts

Xiaolan Zeng, Xiaoyue Huo, Tianle Zhu *, Xiaowei Hong and Ye Sun

School of Space and Environment, Beihang University, Beijing 100191, China; xlzeng@buaa.edu.cn (X.Z.); xyhuo1123@163.com (X.H.); hongxiao86@126.com (X.H.); suny@buaa.edu.cn (Y.S.)
* Correspondence: zhutl@buaa.edu.cn; Tel./Fax: +86-10-8231-4215

Abstract: A series of MnO_x–CeO_2 and MnO_x–TiO_2 catalysts were prepared by a homogeneous precipitation method and their catalytic activities for the NO oxidation in the absence or presence of SO_2 were evaluated. Results show that the optimal molar ratio of Mn/Ce and Mn/Ti are 0.7 and 0.5, respectively. The MnO_x–CeO_2 catalyst exhibits higher catalytic activity and better resistance to SO_2 poisoning than the MnO_x–TiO_2 catalyst. On the basis of Brunauer–Emmett–Teller (BET), X-ray diffraction (XRD), and scanning transmission electron microscope with mapping (STEM-mapping) analyses, it is seen that the MnO_x–CeO_2 catalyst possesses higher BET surface area and better dispersion of MnO_x over the catalyst than MnO_x–TiO_2 catalyst. X-ray photoelectron spectroscopy (XPS) measurements reveal that MnO_x–CeO_2 catalyst provides the abundance of Mn^{3+} and more surface adsorbed oxygen, and SO_2 might be preferentially adsorbed to the surface of CeO_2 to form sulfate species, which provides a protection of MnO_x active sites from being poisoned. In contrast, MnO_x active sites over the MnO_x–TiO_2 catalyst are easily and quickly sulfated, leading to rapid deactivation of the catalyst for NO oxidation. Furthermore, temperature programmed desorption with NO and O_2 (NO + O_2-TPD) and in situ diffuse reflectance infrared transform spectroscopy (in situ DRIFTS) characterizations results show that the MnO_x–CeO_2 catalyst displays much stronger ability to adsorb NO_x than the MnO_x–TiO_2 catalyst, especially after SO_2 poisoning.

Keywords: MnO_x–CeO_2; MnO_x–TiO_2; catalytic oxidation; NO; SO_2

1. Introduction

Nitrogen oxides (NO_x) emitted from stationary and mobile sources are some of the main air pollutants, which cause a variety of serious environmental problems, such as photochemical smog, acid rain, and greenhouse effect [1]. Moreover, NO_x are the primary precursors of haze occurring in China. Therefore, NO_x removal has become the focus of recent environmental protection. The most effective and mature technology is the selective catalytic reduction using ammonia as a reducing agent (NH_3-SCR). However, there still exist some problems, such as high reaction temperature, sophisticated system design, and high operation cost. Additionally, it is possible to cause secondary pollution due to the leakage of ammonia [2].

In order to solve the problems of NH_3-SCR, much attention has been paid to the simultaneous removal of SO_2 and NO_x by chemical absorption. For the absorption operation, the oxidation of NO with low water-solubility to NO_2 is a crucial process because NO accounts for about 95% of NO_x. In general, the oxidation of NO to NO_2 can be realized through gas phase oxidation and liquid phase oxidation. The presence of SO_2 is disadvantageous to NO oxidation in the liquid phase because of the high solubility and oxidizability of SO_2, whereas the oxidation rate of SO_2 is much lower than that of NO in the gas phase [3]. The gas phase oxidation is divided into homogeneous gas phase oxidation and heterogeneous gas-solid catalytic oxidation. Nowadays, catalytic oxidation of NO is potentially

an ideal technology due to its simple operation and low cost, and considerable interest has been put into the investigation of developing catalysts for oxidizing NO into NO_2.

The catalysts for NO oxidation mainly include noble metal catalysts, transition metal catalysts, and molecular sieve catalysts. Noble metal catalysts exhibit high catalytic activity at low temperature, but are limited in industrial applications because of their high cost and poisoning problems [4–9]. Molecular sieve catalysts show certain catalytic activity but they are hydrothermally unstable and susceptible to structure collapse [10]. Transition metal oxides are cheap and also have good catalytic activity and, thus, can be appropriate catalysts for the catalytic oxidation of NO. Among the variety of transition metal catalysts, Co-based and Mn-based catalysts display the best catalytic activity for NO oxidation [11]. However, the applications of Co-based catalysts are retarded due to the toxicity of cobalt although they attract much attention [12–19]. Mn-based catalysts are considered as the promising candidates for NO oxidation to NO_2. Many Mn-based catalysts (e.g., MnO_x/TiO_2 [20–22], $Ce–Mn/TiO_2$ [23], $FeMnO_x/TiO_2$ [24,25]) have been studied. The results show that MnO_x supported on TiO_2 (P25) prepared by deposition-precipitation (DP) method and chemical vapor condensation method exhibits high catalytic activity. Additionally, NO oxidation efficiency can be enhanced by modifying MnO_x/TiO_2 with Ce and Fe. Most recently, many Mn-based catalysts (e.g., Mn–Ce–Ti [26], $MnO_x/CeO_2–ZrO_2$ [27], $MnO_2/TiO_2–Pal$ [28], $Co–Mn/TiO_2$ [29], $Fe_2O_3@MnO_x@CNTs$ [30], and $MnO_2@NiCo_2O_4$ [31]) have also been studied on the selective catalytic reduction of NO_x, and they exhibit good catalytic activities. On the other hand, CeO_2, as a carrier or promoter, also has been studied extensively because of its redox properties and exceptional ability to store and release oxygen. Meanwhile, studies also show that CeO_2 possesses excellent ability to resist SO_2 poisoning [23,32].

In this study, we compared the catalytic activity and resistance to SO_2 poisoning of $MnO_x–CeO_2$ and $MnO_x–TiO_2$ catalysts. The fresh and SO_2 poisoned catalysts were characterized by XRD, BET, STEM-mapping, XPS, NO + O_2-TPD and in situ DRIFTS to clarify the structure-effect relationship.

2. Results and Discussion

2.1. Catalytic Activity Tests

The NO oxidation efficiencies over the $MnO_x–CeO_2$-*x* and $MnO_x–TiO_2$-*y* catalysts are shown in Figure 1a,b, respectively. It can be seen that TiO_2 shows negligible catalytic activity during the reaction temperature range, while CeO_2 has certain catalytic activity for NO oxidation. Nonetheless, the catalytic activity of CeO_2 is lower and the activity temperature is higher, compared with those of $MnO_x–CeO_2$-*x* catalysts. Therefore, MnO_x was the main active component for the catalytic oxidation of NO. In the presence of SO_2, the optimal molar ratio of Mn/Ce and Mn/Ti was 0.7 and 0.5, respectively. Meanwhile, the maximum NO oxidation efficiency of 72% over $MnO_x–CeO_2$-0.7 catalyst is obtained at 325 °C, while that of 62% over $MnO_x–TiO_2$-0.5 catalyst is obtained at 375 °C Therefore, the $MnO_x–CeO_2$-0.7 catalyst has better catalytic activity than the $MnO_x–TiO_2$-0.5 catalyst.
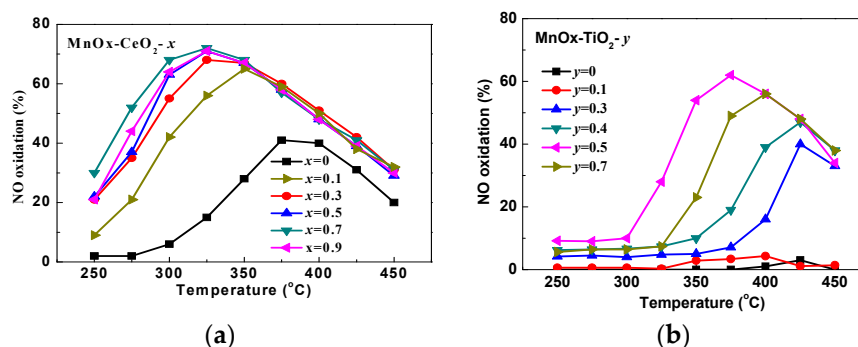

Figure 1. NO oxidation over $MnO_x–CeO_2$-*x* catalysts (**a**) and $MnO_x–TiO_2$-*y* catalysts (**b**). Reaction conditions: 400 ppm NO, 10% O_2, 1% H_2O, 100 ppm SO_2, balanced with N_2; GHSV = 40,000 h^{-1}.

Actually, the catalytic activities of MnO_x–CeO_2-0.7 and MnO_x–TiO_2-0.5 catalysts were also investigated in the absence of SO_2, and the results show that the maximum NO oxidation efficiency of MnO_x–CeO_2-0.7 and MnO_x–TiO_2-0.5 catalysts are 91% and 86% at 300 °C, as shown in Figure 2. Clearly, the presence of SO_2 results in a decrease of NO oxidation efficiency and an increase of the active temperature, especially for the MnO_x–TiO_2-0.5 catalyst. The MnO_x–CeO_2-0.7 catalyst displays better resistance to SO_2 poisoning than the MnO_x–TiO_2-0.5 catalyst.

Figure 2. The effect of SO_2 on NO oxidation over MnO_x–CeO_2-0.7 and MnO_x–TiO_2-0.5 catalysts. Reaction conditions: 400 ppm NO, 10% O_2, 1% H_2O, 100 ppm SO_2 (when used), balanced with N_2; GHSV = 40,000 h^{-1}.

The stability tests for NO oxidation over MnO_x–CeO_2-0.7 and MnO_x–TiO_2-0.5 catalysts were carried out under different temperatures. As shown in Figure 3a, the NO oxidation efficiency of the MnO_x–TiO_2-0.5 catalyst decreases much more rapidly than that of the MnO_x–CeO_2-0.7 catalyst. The catalytic activity of the MnO_x–CeO_2-0.7 catalyst gradually decreases at 300 °C, and maintains almost unchanged within 5 h at 350 °C while it decreases after 5 h. The stability tests without SO_2 over two catalysts were also carried out at 300 °C, and no activity decrease is observed in 20 h (the results are not shown here), which convinces us that the deactivation in Figure 3 is caused by the presence of SO_2. The on-off effect of SO_2 for NO oxidation over MnO_x–CeO_2-0.7 catalyst was investigated. As shown in Figure 3b, when 100 ppm SO_2 are added to the reactants, the NO oxidation efficiency decreases from the initial 80% to 27% after 10 h. After excluding SO_2 from the flue gas, the NO oxidation efficiency only recovers to 32%, which indicates that the poisoning effect of SO_2 is irreversible.
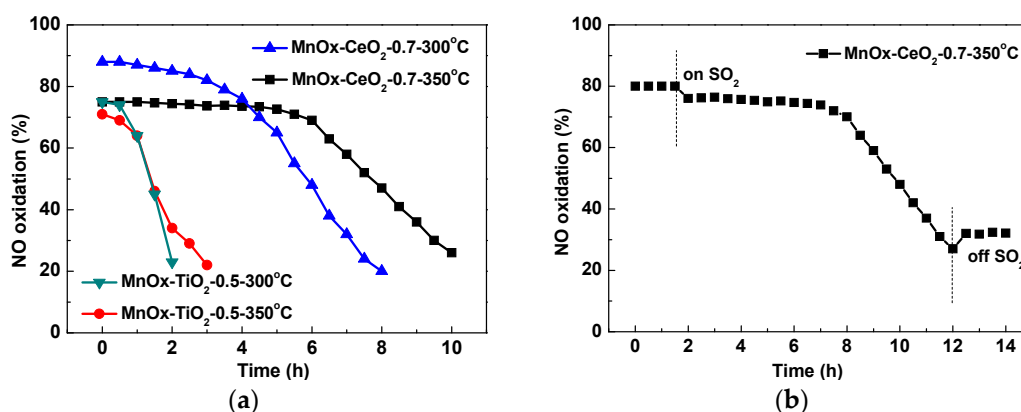

Figure 3. The stability test for NO oxidation over MnO_x–CeO_2-0.7 and MnO_x–TiO_2-0.5 catalysts (**a**); The effect of on-off of SO_2 over MnO_x–CeO_2-0.7 catalyst (**b**). Reaction conditions: 400 ppm NO, 10% O_2, 1% H_2O, 100 ppm SO_2 (when used), balanced with N_2; GHSV = 40,000 h^{-1}.

2.2. XRD and BET Characterizations

Figure 4 presents the XRD patterns of fresh and SO_2 poisoned catalysts. For MnO_x–CeO_2-0.7 catalyst and SO_2 poisoned MnO_x–CeO_2-0.7 catalyst (donated as MnO_x–CeO_2-0.7-S), crystalline phases of CeO_2 can be clearly observed, and very weak signals of Mn_2O_3 are also detected, which indicates that Mn_2O_3 exists in a poor crystal structure. For MnO_x–TiO_2-0.5 catalyst and SO_2 poisoned MnO_x–TiO_2-0.5 catalyst (donated as MnO_x–TiO_2-0.5-S), the stronger diffraction peaks of Mn_2O_3 are observed besides crystalline phases of rutile and anatase TiO_2, which suggests that Mn_2O_3 exists in crystal structure. It is well know that the low crystallinity of MnO_x is favorable for catalytic reaction [20]. Therefore, the higher activity of MnO_x–CeO_2-0.7 catalyst may be partly due to the well dispersion of MnO_x. For all of the samples, the diffraction peaks almost do not change due to SO_2 poisoning.
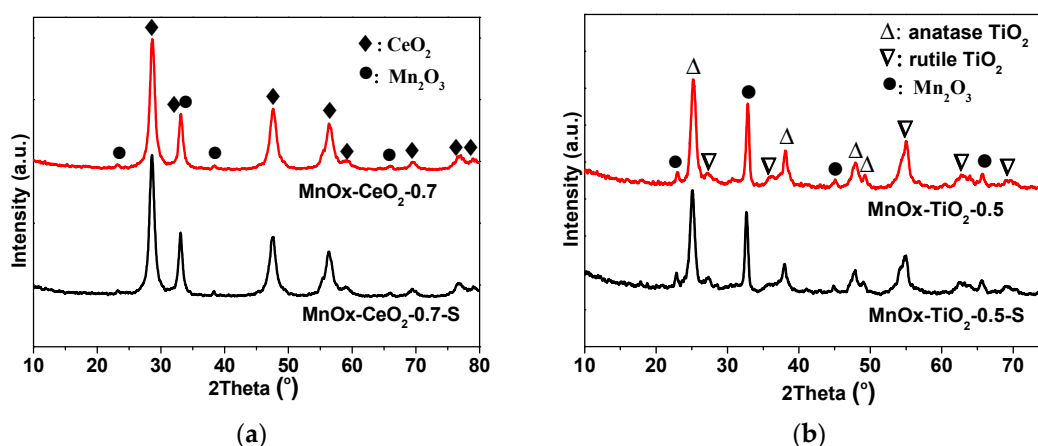

Figure 4. XRD patterns of MnO_x–CeO_2-0.7 and MnO_x–CeO_2-0.7-S catalysts (**a**) and MnO_x–TiO_2-0.5 and MnO_x–TiO_2-0.5-S catalysts (**b**).

The BET surface areas of the catalysts are summarized in Table 1. It can be seen that the specific surface areas of fresh MnO_x–CeO_2-0.7 and MnO_x–TiO_2-0.5 catalysts are 96.30 and 60.21 $m^2 \cdot g^{-1}$. Compared to catalytic performance, it is consistent with that of BET surface. Furthermore, it is worth noting that the BET specific surface areas of SO_2 poisoned catalysts decrease to 67.92 (MnO_x–CeO_2-0.7) $m^2 \cdot g^{-1}$ and 39.71 (MnO_x–TiO_2-0.5) $m^2 \cdot g^{-1}$, which may be caused by the formation of sulfate species.

Table 1. BET surface area of the catalysts.

Catalysts	Surface Area (m^2/g)
MnO_x–CeO_2-0.7	93.17
MnO_x–CeO_2-0.7-S	67.92
MnO_x–TiO_2-0.5	60.21
MnO_x–TiO_2-0.5-S	39.71

2.3. STEM-Mapping Analysis

Figure 5 presents STEM images and their mapping analysis of fresh MnO_x–CeO_2-0.7 and MnO_x–TiO_2-0.5 catalysts. For the MnO_x–CeO_2-0.7 catalyst, Mn, Ce, O evenly disperses on the scanning area, which indicates excellent distribution of MnO_x and CeO_2. For the MnO_x–TiO_2-0.5 catalyst, however, many of the Mn and O atoms appear on the scanning area, while few Ti atoms are seen. Therefore, we deduce that TiO_2 cannot disperse MnO_x well, which can lead to low catalytic activity of the MnO_x–TiO_2-0.5 catalyst.
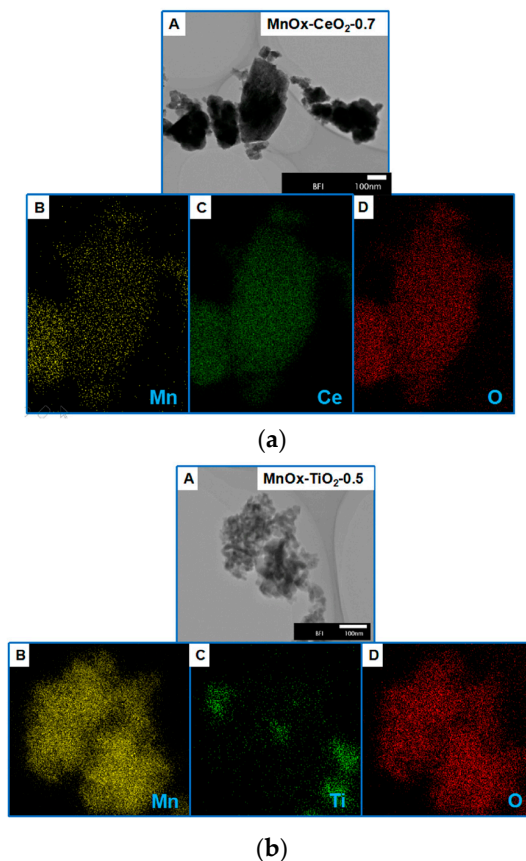
(a)

(b)

Figure 5. STEM images and their mapping analyses of MnO$_x$–CeO$_2$-0.7 catalyst (**a**) and MnO$_x$–TiO$_2$-0.5 catalyst (**b**). (**A**) STEM images of MnO$_x$–CeO$_2$-0.7 or MnO$_x$–TiO$_2$-0.5 catalysts; (**B**) Mn; (**C**) Ce or Ti; and (**D**) O.

2.4. XPS Analysis

XPS analysis was performed to identify the surface component and chemical states of fresh and SO$_2$ poisoned catalysts. Surface atomic concentration and ratio are summarized in Table 2, and XPS spectra of Mn 2p, O 1s, Ce 3d, and Ti 2p of all catalysts are displayed in Figure 6. Through the deconvolution of the spectra, two main peaks due to Mn 2p$_{1/2}$ and Mn 2p$_{3/2}$ are observed. The Mn 2p$_{3/2}$ profiles are fitted with the Mn^{2+}, Mn^{3+}, and Mn^{4+}, characterized by the binding energy at about 641.1 eV, 642.5 eV, and 645.1 eV [33], respectively. Previous studies [20,22,34] have shown that Mn$_2$O$_3$ has a higher catalytic activity than MnO$_2$ for NO oxidation. Cimino et al. [35] attributed the higher activity of Mn^{3+} than Mn^{4+} for CO catalytic oxidation to the weaker Mn^{3+}–O bond. Similarly, it can be deduced that the weaker Mn^{3+}–O bonds will also favor the catalytic oxidation of NO since the Mn^{3+}–O bond is easily broken, thus, promoting the generation and release of the NO$_2$ oxidation product. As shown in Table 2, all catalysts contain high concentration of Mn^{3+}. Corresponding to the high catalytic activity of catalyst, it, combining with XRD analysis results, can be also speculated that Mn^{3+} has higher catalytic activity than Mn^{2+} and Mn^{4+} for NO oxidation. The Ce 3D XPS spectra can be separated into eight peaks: u_0 (900.6 eV), u_1 (902.4eV), u_2 (907.9 eV), u_3 (916.6 eV), v_0 (881.9 eV), v_1 (884.4 eV), v_2 (889.1 eV), and v_3 (898.1 eV) [36]. The bands labeled as u_1 and v_1 are attributed to Ce^{3+} species, and the other six peaks are assigned to Ce^{4+} species. The ratio of Ce^{3+}/(Ce^{3+} + Ce^{4+}) can be estimated by the formula [37]:
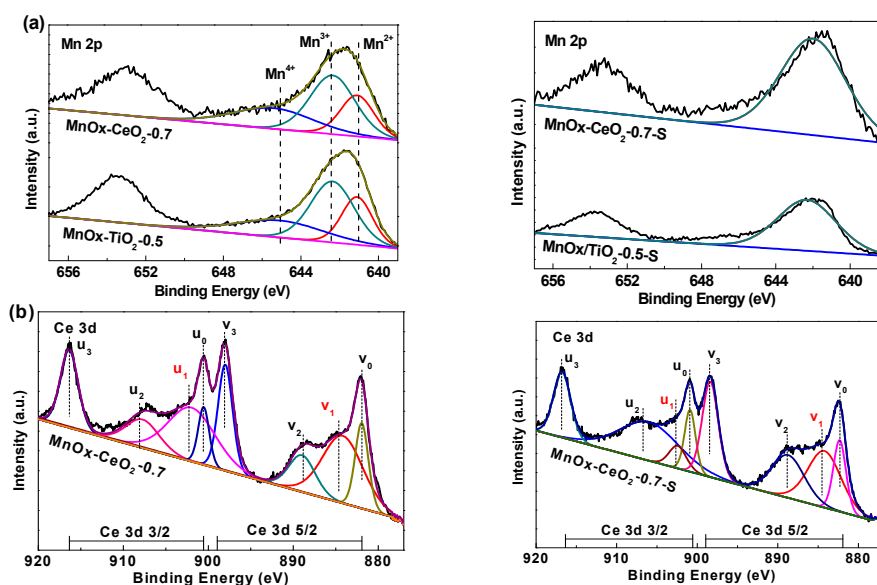
$$Ce^{3+}(\%) = \frac{S_{u_1} + S_{v_1}}{\sum\limits_{i=0}^{3}(S_{u_i} + S_{v_i})} \times 100\%$$

Table 2. Surface atomic distributions of the catalysts by XPS.

Catalysts	Atomic Concentration (%)			Surface Atomic Ratio (%)		
	Mn	Ce or Ti	O	$Mn^{3+}/(Mn^{2+} + Mn^{3+} + Mn^{4+})$	$Ce^{3+}/(Ce^{3+} + Ce^{4+})$ or $Ti^{3+}/(Ti^{3+} + Ti^{4+})$	$O_\alpha/(O_\alpha + O_\beta)$
MnO_x–CeO_2-0.7	5.6	26.4	68.0	46.42	41.46	33.4
MnO_x–CeO_2-0.7-S	5.4	19.7	70.6	-	25.2	50.3
MnO_x–TiO_2-0.5	13.6	18.8	67.6	47.31	87.9	25.6
MnO_x–TiO_2-0.5-S	9.4	13.3	74.4	-	87.1	55.8

It is well known that Ce^{3+} species can make charge imbalance and create oxygen vacancies via the shift from Ce^{3+} to Ce^{4+}, which leads to the increase of surface adsorbed oxygen ($Ce^{3+} \rightarrow Ce^{4+} + e^-$, $O_2 + e^- \rightarrow O_2^-$) [38]. For the catalytic oxidation of NO, surface adsorbed oxygen plays a significant role because of its mobility and redox performance [39]. As listed in Table 2, the Ce^{3+} concentration can reach about 41.6%. Figure 6c displays the O 1s XPS spectra of all samples, two distinct bands are obtained. The one peak O_β in the range of 528–530 eV belongs to lattice oxygen and the other peak O_α with binding energy of 530–532 eV corresponds to weakly surface adsorbed oxygen [18]. From Table 2, it can be seen that the O_α concentration over MnO_x–CeO_2-0.7 catalyst is higher than that over MnO_x–TiO_2-0.5 catalyst, which is attributed to the presence of Ce^{3+} species.

On the other hand, the Mn concentration of the MnO_x–CeO_2-0.7-S catalyst is almost the same to that of the fresh MnO_x–CeO_2-0.7 catalyst, while the Mn concentration of MnO_x–TiO_2-0.5 catalyst and the Ce concentration of MnO_x–CeO_2-0.7 catalyst decrease from 13.6% to 9.4% and from 26.4% to 19.7%, respectively, because of SO_2 poisoning, which is attributed that the MnO_x over MnO_x–TiO_2-0.5-S catalyst and CeO_2 over MnO_x–CeO_2-0.7-S catalyst are partly covered with sulfate species [36]. Meanwhile, the ratio of $Ce^{3+}/(Ce^{3+} + Ce^{4+})$ of the MnO_x–CeO_2-0.7 catalyst also decreases from 41.6% to 25.2%, which indicates that cerium(IV) sulfate may be formed on the catalyst surface [40]. Therefore, we can deduce that SO_2 might be preferentially adsorbed to the surface of CeO_2 to form sulfate species, lessening the sulfation of MnO_x active sites. It was also reported by Jin and co-workers [32] that the presence of CeO_2 might partially prevent MnO_x active sites from being sulfated. Waqif [41] investigated the adsorption of SO_2 on CeO_2–Al_2O_3, and concluded that ceria was a basic material for SO_2 adsorption. Figure 4d shows the Ti 2p XPS spectra, four peaks are formed, referred to as Ti^{3+} at 458.3 eV, 464.1 eV, and Ti^{4+} at 459.8 eV, 466.1 eV, respectively [23]. Though the Ti^{3+} concentration is pretty high, it still cannot improve the resistance to SO_2 poisoning.

Figure 6. *Cont.*
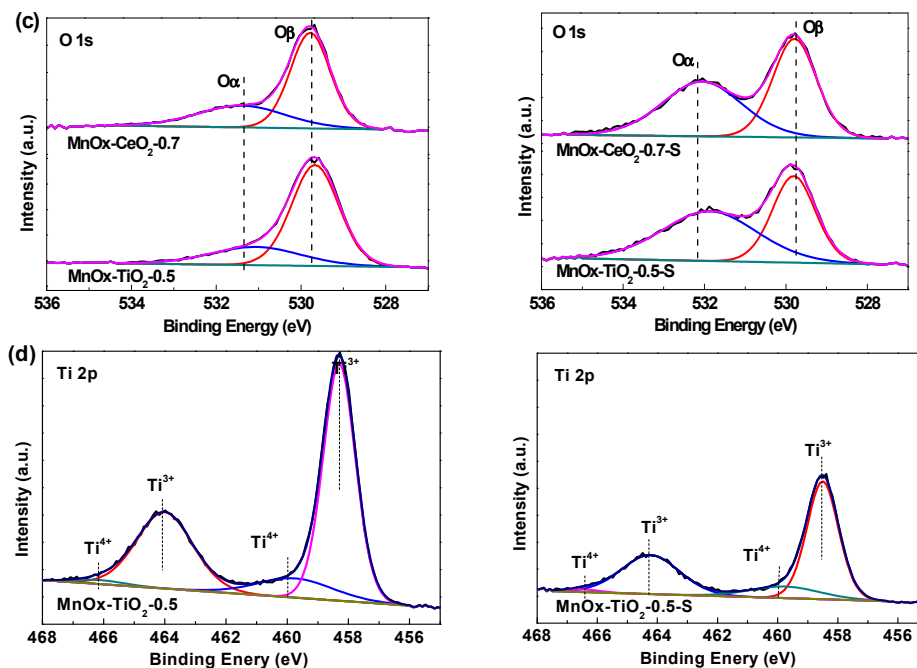
Figure 6. XPS spectra of the catalysts. (**a**) Mn 2p; (**b**) Ce 3d; (**c**) O 1s; and (**d**) Ti 2p.

2.5. NO + O_2-TPD and In Situ DRIFTS Analyses

The adsorption behavior of the catalyst is considered a crucial step in a catalytic oxidation reaction. Therefore, NO + O_2-TPD experiments were conducted to explore the NO_x adsorption ability over MnO_x–CeO_2-0.7 and MnO_x–TiO_2-0.5 catalysts. As shown in Figure 7a,b, the NO and NO_2 curves over MnO_x–CeO_2-0.7 and MnO_x–TiO_2-0.5 catalysts are observed. For the MnO_x–CeO_2-0.7 catalyst, the desorption peak at about 240 °C is assigned to nitrosyl species [42], the desorption peak in the temperature range of 350–450 °C can be ascribed to the decomposition of strong adsorption species such as nitrate on catalyst surface [43]. For the MnO_x–TiO_2-0.5 catalyst, three major desorption peaks at 80, 180, and 320 °C are observed, which may be attributed to desorption of molecularly-adsorbed NO and NO_2, nitrosyl species and desorption of nitrate species, respectively [42,44,45]. It is obvious that the total amount of NO_x desorbed from MnO_x–CeO_2-0.7 catalyst is remarkably larger than that of the MnO_x–TiO_2-0.5 catalyst, indicating stronger adsorption and oxidation abilities on the surface of the MnO_x–CeO_2-0.7 catalyst.

In order to understand the NO_x adsorption behaviors and SO_2 poisoning process, in situ DRIFTS measurements over MnO_x–CeO_2-0.7 and MnO_x–TiO_2-0.5 catalysts were carried out at 350 °C. Figure 7c,d shows the NO-O_2 co-adsorption accompanied by SO_2 adsorption. After introducing NO + O_2, for the MnO_x–CeO_2-0.7 catalyst, the bands at 1593, 1566, 1540, 1242, and 1212 cm^{-1} are detected. All of the bands' intensities gradually increase with the adsorption time until reaching their highest intensities and remain stable after about 40 min. The bands at 1566, 1540, and 1212–1242 cm^{-1} are assigned to bidentate nitrate, monodentate nitrate, and bridge nitrate, respectively [46]. A very weak band at 1593 cm^{-1} is due to the adsorption of NO_2 [47]. For the MnO_x–TiO_2-0.5 catalyst, the bands attributed to monodentrate nitrate (1235 cm^{-1}), bidentrate nitrate (1548 cm^{-1}), and bridge nitrate (1608 cm^{-1}) are observed [44]. The change trend of these bands' intensities is similar to those over the MnO_x–CeO_2-0.7 catalyst. However, it is obvious that all of the adsorption bands' intensities of the MnO_x–TiO_2-0.5 catalyst are significantly lower than those of the MnO_x–CeO_2-0.7 catalyst, which is probably one of the reasons that the MnO_x–CeO_2-0.7 catalyst has better activity than the MnO_x–TiO_2-0.5 catalyst in the absence of SO_2.
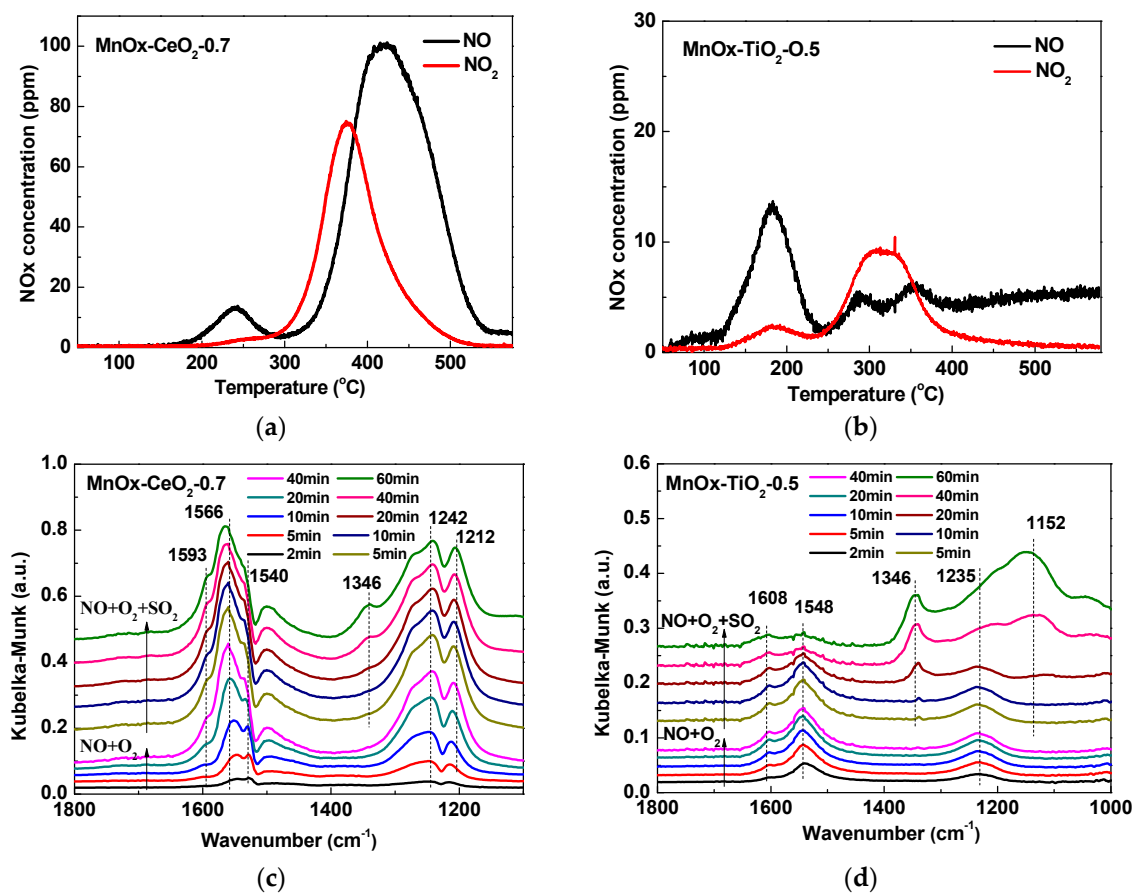
Figure 7. NO + O_2-TPD profiles of the MnO_x–CeO_2-0.7 catalyst (**a**) and the MnO_x–TiO_2-0.5 catalyst (**b**); in situ DRIFTS spectra of MnO_x–CeO_2-0.7 catalyst (**c**); and MnO_x–TiO_2-0.5 catalyst (**d**) at 350 °C.

In the following, 100 ppm SO_2 was added to the reaction system. It can be seen from Figure 7c that a new band at 1346 cm^{-1} appears over the MnO_x–CeO_2-0.7 catalyst and the intensity grows with time. Similarly, the new peaks at 1346 cm^{-1} and 1152 cm^{-1} are also observed over the MnO_x–TiO_2-0.5 catalyst and their intensities rise rapidly with the reaction time. The band at 1346 cm^{-1} is due to the v (S=O) vibration of surface sulfate species, and the band at 1152 cm^{-1} can be ascribed to sulfate species [48]. Moreover, it can be noted that all the adsorption bands' intensities almost remain unchanged within 10 min and the bands' intensities of monodentrate and bidentrate nitrate slightly decrease for the MnO_x–CeO_2-0.7 catalyst. However, the bands' intensities at 1608 cm^{-1} and 1548 cm^{-1} drop rapidly with time and the peak of monodentrate nitrate almost vanishes after 60 min for the MnO_x–TiO_2-0.5 catalyst. The results confirm that SO_2 has little influence on NO_x adsorption over the MnO_x–CeO_2-0.7 catalyst, while there is strongly competitive adsorption between SO_2 and NO_x over the MnO_x–TiO_2-0.5 catalyst in a certain reaction time. Tang et al. [49] reported the mechanism of catalytic oxidation of NO over Mn-based catalysts that NO firstly adsorbed on Mn sites to form nitrosyls, and then were oxidized to nitrates, which decomposed to the final product, NO_2.

According to the DRIFTS results and the mechanism, we further deduce that SO_2 preferentially combines with CeO_2 to form sulfate species, and MnO_x active sites are exposed to the surface to adsorb NO_x over the MnO_x–CeO_2-0.7 catalyst. Whereas MnO_x active sites are sulfated so seriously that the MnO_x–TiO_2-0.5 catalyst has no ability to adsorb NO_x, leading to low catalytic activity. The results are consistent with XPS analysis. Moreover, the formation of sulfate species is irreversible and sulfate species occupied the sites for NO oxidation permanently. Through the above analysis, it is sufficient to prove that the catalytic activity and resistance to SO_2 poisoning of MnO_x–CeO_2 catalysts are better than MnO_x–TiO_2 catalysts.

3. Materials and Methods

3.1. Catalyst Preparation

A series of MnO$_x$–CeO$_2$-x and MnO$_x$–TiO$_2$-y catalysts, where x and y are the molar ratio of Mn/Ce and Mn/Ti, respectively, were prepared by homogeneous precipitation method. Take MnO$_x$–CeO$_2$-0.7 for example, 13.02 g Ce(NO$_3$)$_3$·6H$_2$O and 7.15 g Mn(NO$_3$)$_2$ (50% solution) were firstly added to 100 mL deionized water and stirred for 2 h. Excessive urea aqueous solution was added into the mixed solution under stirring. Then, the mixed solution was stirred for 12 h at 90 °C. In order to make Mn precipitate completely, an appropriate amount of ammonia solution were added into the mixed solution until the pH value was 9.5. The precipitate was collected by filtration and washed with deionized water, followed by drying at 110 °C overnight and subsequently calcination at 500 °C for 4 h in the air atmosphere. MnO$_x$–TiO$_2$-y catalysts were prepared by similar process with MnO$_x$–CeO$_2$-x catalysts. The difference is that tetrabutyl titanate was firstly dissolved in ethanol. Finally, the catalysts were crushed and sieved to 40–60 mesh for activity test.

3.2. Catalytic Activity Measurement

The catalytic activity was evaluated in a quartz U-tube fixed-bed flow reactor (i.d. 13 mm) from 450–250 °C. The test data was recorded after the reaction for 40 min at each temperature. The reaction gas consisted of 400 ppm NO, 10% O$_2$, 1% H$_2$O, 100 ppm SO$_2$ (when used), and balanced with N$_2$. The total flow rate was fixed at 2 L/min, which is corresponded to a gas hourly space velocity (GHSV) of 40,000 h^{-1}. The concentrations of NO, NO$_2$, O$_2$, and SO$_2$ were analyzed by a flue gas analyzer (Testo 350, Testo AG, Schwarzwald, Germany). The NO oxidation efficiency was calculated by the following equation:

$$\text{NO oxidation } (\%) = \frac{[\text{NO}]_{\text{inlet}} - [\text{NO}]_{\text{outlet}}}{[\text{NO}]_{\text{inlet}}} \times 100\%$$

3.3. Catalyst Characterization

The XRD patterns were recorded by powder X-ray diffractometer (XRD-600) with Cu Kα radiation (λ = 1.54 Å). The samples were scanned at 2θ ranging from 10° to 80° with a scan speed of 6° min^{-1}. BET Surface areas of the catalysts were determined by N$_2$ adsorption-desorption isotherms at −196 °C using specific surface area and porosity analyzer (NOVA 2200, Quantachrome, Boynton Beach, FL, USA). The samples were degassed under vacuum at 300 °C for 4 h. The STEM-mapping analysis was performed using a transmission electron microscope (JEM-2100F, JEOL, Tokyo, Japan) to observe distribution of metal oxides. The surface chemical states of catalysts were tested by X-ray photoeletron spectra (PHI Quantro SXM$^{\text{TM}}$, ULVAC-PHI, Kanagawa, Japan) using an Al Kα X-ray source (1486.7 eV) at 15 kV and 25 W with the binding energy calibrated by C 1s at 284.8 eV.

The NO + O$_2$-TPD experiments were performed in a quartz reactor with a FTIR spectrometer (MultiGas$^{\text{TM}}$ 2030 HS). Prior to the tests, the samples (200 mg) were pretreated in 10% O$_2$/N$_2$ (500 mL/min) at 500 °C 0.5 h followed by cooling down to 350 °C. The catalysts were exposed to 400 ppm NO, 10% O$_2$, N$_2$ at 350 °C for 40 min, and then cooled down to 50 °C rapidly with N$_2$ purging. Subsequently, the catalysts were again heated from 50–600 °C with a rate of 10 °C/min in N$_2$.

In situ DRIFTS investigations were performed using a Nicolet 6700 spectrometer at 4 cm^{-1} resolution with 64 co-added scans. Prior to adsorption experiments, the catalysts were pretreated at 500 °C for 0.5 h in N$_2$ (100 mL·min^{-1}) to eliminate the physisorbed water and other impurities. Then the samples were cooled down to 350 °C. After the background was subtracted, the samples were firstly exposed to certain reaction gas mixtures containing 400 ppm NO, 10% O$_2$, 1% H$_2$O, and balanced with N$_2$ (total flow 100 mL·min^{-1}) for 40 min. Subsequently, the catalysts were treated under 400 ppm NO, 10% O$_2$, 1% H$_2$O, 100 ppm SO$_2$, and balanced with N$_2$ for 60 min, and the in situ DRIFTS spectra were recorded in the range of 4000–900 cm^{-1}.

4. Conclusions

In this work, catalytic oxidation of NO over MnO_x–CeO_2 and MnO_x–TiO_2 catalysts were studied in the absence or presence of SO_2. The optimal molar ratio of Mn/Ce and Mn/Ti are 0.7 and 0.5, respectively. MnO_x–CeO_2 catalyst gives the highest NO oxidation efficiency of 72% at 325 °C and the NO oxidation efficiency maintained unchanged in 5 h in the presence of 100 ppm SO_2 at 350 °C, while MnO_x–TiO_2 catalyst only yields 62% NO oxidation efficiency at 375 °C, and exhibits poor catalytic activity below 325 °C. MnO_x–CeO_2 catalysts exhibit better catalytic activity and resistance to SO_2 poisoning than that of MnO_x–TiO_2 catalysts, which is attributed that MnO_x–CeO_2 catalyst possesses higher surface area, better dispersion of MnO_x and stronger NO_x adsorption oxidation ability, offers the abundance of Mn^{3+} and more surface adsorbed oxygen, and SO_2 might be preferentially adsorbed to the surface of CeO_2 to form sulfate species, lessening the sulfation of MnO_x sites.

Author Contributions: Tianle Zhu conceived and designed the experiments; Xiaolan Zeng and Xiaoyue Huo performed the experiments; Xiaolan Zeng, Xiaoyue Huo, Xiaowei Hong and Ye Sun analyzed the data; Xiaolan Zeng, Xiaoyue Huo and Tianle Zhu wrote the paper.

Conflicts of Interest: The authors declare no conflict of interest.

References

1. Zhu, J.; Thomas, A. Perovskite-Type Mixed Oxides as Catalytic Material for NO Removal. *Appl. Catal. B Environ.* **2009**, *92*, 225–233. [CrossRef]

2. Skalska, K.; Miller, J.S.; Ledakowicz, S. Trends in NO_x abatement: A review. *Sci. Total Environ.* **2010**, *408*, 3976–3989. [CrossRef] [PubMed]

3. Guo, S.; Lv, L.; Zhang, J.; Chen, X.; Tong, M.; Kang, W.; Zhou, Y.; Lu, J. Simultaneous removal of SO_2 and NO_x with ammonia combined with gas-phase oxidation of NO using ozone. *Chem. Ind. Chem. Eng. Q.* **2015**, *21*, 305–310. [CrossRef]

4. Dawody, J.; Skoglundh, M.; Fridell, E. The effect of metal oxide additives (WO_3, MoO_3, V_2O_5, Ga_2O_3) on the oxidation of NO and SO_2 over Pt/Al_2O_3 and $Pt/BaO/Al_2O_3$ catalysts. *J. Mol. Catal. A Chem.* **2004**, *209*, 215–225. [CrossRef]

5. Crocoll, M.; Kureti, S.; Weisweiler, W. Mean field modeling of NO oxidation over Pt/Al_2O_3 catalyst under oxygen-rich conditions. *J. Catal.* **2005**, *229*, 480–489. [CrossRef]

6. Fujii, T.; Sato, R. Characterization and activity of Pd-modified TiO_2 catalysts for photocatalytic oxidation of NO in gas phase. *J. Hazard. Mater.* **2009**, *164*, 542–548.

7. Kaneeda, M.; Iizuka, H.; Hiratsuka, T.; Shinotsuka, N.; Arai, M. Improvement of thermal stability of NO oxidation Pt/Al_2O_3 catalyst by addition of Pd. *Appl. Catal. B* **2009**, *90*, 564–569. [CrossRef]

8. Boubnov, A.; Dahl, S.; Johnson, E.; Molina, A.P.; Simonsen, S.B.; Cano, F.M.; Helveg, S.; Lemus-Yegres, L.J.; Grunwaldt, J.D. Structure–activity relationships of Pt/Al_2O_3 catalysts for CO and NO oxidation at diesel exhaust conditions. *Appl. Catal. B* **2012**, *126*, 315–325. [CrossRef]

9. Khosravi, M.; Sola, C.; Abedi, A.; Hayes, R.E.; Epling, W.S.; Votsmeier, M. Oxidation and selective catalytic reduction of NO by propene over Pt and Pt:Pd diesel oxidation catalysts. *Appl. Catal. B* **2014**, *147*, 264–274. [CrossRef]

10. Berggrund, M.; Ingelsten, H.H.; Skoglundh, M.; Palmqvist, A.E.C. Influence of Synthesis Conditions for ZSM-5 on the Hydrothermal Stability of Cu-ZSM-5. *Catal. Lett.* **2009**, *130*, 79–85. [CrossRef]

11. Karlsson, H.T.; Rosenberg, H.S. Flue gas denitrification. Selective catalytic oxidation of NO to NO_2. *Ind. Eng. Chem. Process Des. Dev.* **1984**, *23*, 808–814. [CrossRef]

12. Kantcheva, M.; Vakkasoglu, A.S. Cobalt supported on zirconia and sulfated zirconia I.: FT-IR spectroscopic characterization of the NO_x species formed upon NO adsorption and NO/O_2 coadsorption. *J. Catal.* **2004**, *223*, 352–363. [CrossRef]

13. Qiang, W.; Park, S.Y.; Jin, S.C.; Chung, J.S. $Co/K_xTi_2O_5$ catalysts prepared by ion exchange method for NO oxidation to NO_2. *Appl. Catal. B* **2008**, *79*, 101–107.

14. Irfan, M.F.; Sang, D.K.; Goo, J.H. Co_3O_4 based catalysts for NO oxidation and NO_x reduction in fast SCR process. *Appl. Catal. B* **2008**, *78*, 267–274. [CrossRef]

15. Wang, H.; Wang, J.; Wu, Z.; Liu, Y. NO Catalytic Oxidation Behaviors over CoO_x/TiO_2 Catalysts Synthesized by Sol–Gel Method. *Catal. Lett.* **2010**, *134*, 295–302. [CrossRef]

16. Shang, D.; Cai, W.; Zhao, W.; Bu, Y.; Zhong, Q. Catalytic Oxidation of NO to NO_2 Over Co–Ce–Zr Solid Solutions: Enhanced Performance of Ce–Zr Solid Solution by Co. *Catal. Lett.* **2014**, *144*, 538–544. [CrossRef]

17. Shang, D.; Zhong, Q.; Cai, W. Influence of the preparation method on the catalytic activity of $Co/Zr_{1-x}Ce_xO_2$ for NO oxidation. *J. Mol. Catal. A Chem.* **2015**, *399*, 18–24. [CrossRef]

18. Shang, D.; Zhong, Q.; Cai, W. High performance of NO oxidation over Ce–Co–Ti catalyst: The interaction between Ce and Co. *Appl. Surf. Sci.* **2015**, *325*, 211–216. [CrossRef]

19. Yu, Y.; Zhong, Q.; Cai, W.; Ding, J. Promotional effect of N-doped CeO_2 supported CoO_x catalysts with enhanced catalytic activity on NO oxidation. *J. Mol. Catal. A Chem.* **2015**, *398*, 344–352. [CrossRef]

20. Wu, Z.; Tang, N.; Ling, X.; Yue, L.; Wang, H. MnO_x/TiO_2 composite nanoxides synthesized by deposition-precipitation method as a superior catalyst for NO oxidation. *J. Colloid Interface Sci.* **2010**, *352*, 143–148. [CrossRef] [PubMed]

21. Park, E.; Chin, S.; Jeong, J.; Jurng, J. Low-temperature NO oxidation over Mn/TiO_2 nanocomposite synthesized by chemical vapor condensation: Effects of Mn precursor on the surface Mn species. *Micropor. Mesopor. Mater.* **2012**, *163*, 96–101. [CrossRef]

22. An, Z.; Zhuo, Y.; Xu, C.; Chen, C. Influence of the TiO_2 crystalline phase of MnO_x/TiO_2 catalysts for NO oxidation. *Chin. J. Catal.* **2014**, *35*, 120–126. [CrossRef]

23. Li, X.; Zhang, S.; Jia, Y.; Liu, X.; Zhong, Q. Selective catalytic oxidation of NO with O_2 over Ce-doped MnO_x catalysts. *J. Nat. Gas Chem.* **2012**, *21*, 17–24. [CrossRef]

24. Zhang, M.; Li, C.; Qu, L.; Fu, M.; Zeng, G.; Fan, C.; Ma, J.; Zhan, F. Catalytic oxidation of NO with O_2 over $FeMnO_x/TiO_2$: Effect of iron and manganese oxides loading sequences and the catalytic mechanism study. *Appl. Surf. Sci.* **2014**, *300*, 58–65. [CrossRef]

25. Liu, L.; Gao, X.; Zheng, C.; Zhu, X.; Luo, Z.; Ni, M.; Cen, K.; Liu, L.; Ni, M.; Cen, K. Study of the Promotion Effect of Iron on Supported Manganese Catalysts for NO Oxidation. *Aerosol Air Qual. Res.* **2014**, *14*, 1038–1046. [CrossRef]

26. Liu, Z.; Zhu, J.; Li, J.; Ma, L.; Woo, S.I. Novel Mn–Ce–Ti mixed-oxide catalyst for the selective catalytic reduction of NO_x with NH_3. *ACS Appl. Mater. Interfaces* **2014**, *6*, 14500–14508. [CrossRef] [PubMed]

27. Gao, R.; Zhang, D.; Maitarad, P.; Shi, L.; Rungrotmongkol, T.; Li, H.; Zhang, J.; Cao, W. Morphology-Dependent Properties of MnO_x/ZrO_2–CeO_2 Nanostructures for the Selective Catalytic Reduction of NO with NH_3. *J. Phys. Chem. C* **2013**, *117*, 10502–10511. [CrossRef]

28. Luo, S.; Zhou, W.; Xie, A.; Wu, F.; Yao, C.; Li, X.; Zuo, S.; Liu, T. Effect of MnO_2 polymorphs structure on the selective catalytic reduction of NO_x with NH_3 over TiO_2-Palygorskite. *Chem. Eng. J.* **2016**, *286*, 291–299. [CrossRef]

29. Hu, H.; Cai, S.; Li, H.; Huang, L.; Shi, L.; Zhang, D. Mechanistic aspects of $deNO_x$ processing over TiO_2 supported Co-Mn oxide catalysts: Structure-activity relationships and in situ DRIFTs analysis. *ACS Catal.* **2015**, *5*, 6069–6077. [CrossRef]

30. Cai, S.; Hu, H.; Li, H.; Shi, L.; Zhang, D. Design of multi-shell Fe_2O_3@MnO_x@CNTs for the selective catalytic reduction of NO with NH: Improvement of catalytic activity and SO tolerance. *Nanoscale* **2016**, *8*, 3588–3598. [CrossRef] [PubMed]

31. Liu, Y.; Xu, J.; Li, H.; Cai, S.; Hu, H.; Fang, C.; Shi, L.; Zhang, D. Rational design and in situ fabrication of MnO_2@$NiCo_2O_4$ nanowire arrays on Ni foam as high-performance monolith $deNO_x$ catalysts. *J. Mater. Chem. A* **2015**, *3*, 11543–11553. [CrossRef]

32. Jin, R.; Yue, L.; Yan, W.; Cen, W.; Wu, Z.; Wang, H.; Weng, X. The role of cerium in the improved SO_2 tolerance for NO reduction with NH_3 over Mn–Ce/TiO_2 catalyst at low temperature. *Appl. Catal. B* **2014**, *148–149*, 582–588. [CrossRef]

33. Lu, X.; Song, C.; Jia, S.; Tong, Z.; Tang, X.; Teng, Y. Low-temperature selective catalytic reduction of NO_x with NH_3 over cerium and manganese oxides supported on TiO_2-graphene. *Chem. Eng. J.* **2015**, *260*, 776–784. [CrossRef]

34. Atribak, I.; Bueno-López, A.; García-García, A.; Navarro, P.; Frías, D.; Montes, M. Catalytic activity for soot combustion of birnessite and cryptomelane. *Appl. Catal. B* **2010**, *93*, 267–273. [CrossRef]

35. Cimino, A.; Indovina, V. Catalytic activity of Mn^{3+} and Mn^{4+} ions dispersed in MgO for CO oxidation. *J. Catal.* **1974**, *33*, 493–496. [CrossRef]

36. Xiong, Y.; Tang, C.; Yao, X.; Zhang, L.; Li, L.; Wang, X.; Deng, Y.; Gao, F.; Dong, L. Effect of metal ions doping ($M = Ti^{4+}$, Sn^{4+}) on the catalytic performance of MnO_x/CeO_2 catalyst for low temperature selective catalytic reduction of NO with NH_3. *Appl. Catal. A Gen.* **2015**, *495*, 206–216. [CrossRef]

37. Larsson, P.O.; Andersson, A. Complete Oxidation of CO, Ethanol, and Ethyl Acetate over Copper Oxide Supported on Titania and Ceria Modified Titania. *J. Catal.* **1998**, *179*, 72–89. [CrossRef]

38. Wei, C.; Qin, Z.; Wei, Z. Solvent effects on formation of Cr-doped $Ce_{0.2}Zr_{0.8}O_2$ synthesized with cinnamic acid and their catalysis in oxidation of NO. *Chem. Eng. J.* **2014**, *246*, 328–336.

39. Jing, L.; Xu, Z.; Sun, X.; Shang, J.; Cai, W. The surface properties and photocatalytic activities of ZnO ultrafine particles. *Appl. Surf. Sci.* **2001**, *180*, 308–314. [CrossRef]

40. Wu, X.D.; Li, H.R.; Liu, S.; Weng, D. Sulfur poisoning and regeneration of $MnO_x–CeO_2–Al_2O_3$ catalyst for soot oxidation. *J. Rare Earths* **2012**, *30*, 659–664. [CrossRef]

41. Waqif, M.; Pieplu, A.; Saur, O.; Lavalley, J.C.; Blanchard, G. Use of $CeO_2–Al_2O_3$ as a SO_2 sorbent. *Solid State Ion.* **1997**, *95*, 163–167. [CrossRef]

42. Yang, N.Z.; Guo, R.T.; Tian, Y.; Pan, W.G.; Chen, Q.L.; Wang, Q.S.; Lu, C.Z.; Wang, S.X. The enhanced performance of ceria by HF treatment for selective catalytic reduction of NO with NH_3. *Fuel* **2016**, *179*, 305–311. [CrossRef]

43. Wang, W.H.; Li, W.; Guo, R.T.; Chen, Q.L.; Wang, Q.S.; Pan, W.G.; Hu, G.X. A $CeFeO_x$ catalyst for catalytic oxidation of NO to NO_2. *J. Rare Earths* **2016**, *34*, 876–881. [CrossRef]

44. Zhao, B.; Ran, R.; Wu, X.; Weng, D.; Wu, X.; Huang, C. Comparative study of Mn/TiO_2 and Mn/ZrO_2 catalysts for NO oxidation. *Catal. Commun.* **2014**, *56*, 36–40. [CrossRef]

45. Shen, M.; Zhao, Z.; Chen, J.; Su, Y.; Wang, J.; Wang, X. Effects of calcium substitute in $LaMnO_3$ perovskites for NO catalytic oxidation. *J. Rare Earths* **2013**, *31*, 119–123. [CrossRef]

46. Liu, F.; He, H.; Ding, Y.; Zhang, C. Effect of manganese substitution on the structure and activity of iron titanate catalyst for the selective catalytic reduction of NO with NH_3. *Appl. Catal. B* **2009**, *93*, 3760–3769. [CrossRef]

47. And, G.Q.; Yang, R.T. Characterization and FTIR Studies of $MnO_x–CeO_2$ Catalyst for Low-Temperature Selective Catalytic Reduction of NO with NH_3. *J. Phys. Chem. B* **2004**, *108*, 15738–15747.

48. Jiang, B.Q.; Wu, Z.B.; Liu, Y.; Lee, S.C.; Ho, W.K. DRIFT Study of the SO_2 Effect on Low-Temperature SCR Reaction over $Fe-Mn/TiO_2$. *J. Phys. Chem. C* **2010**, *114*, 4961–4965. [CrossRef]

49. Tang, N.; Liu, Y.; Wang, H.; Wu, Z. Mechanism Study of NO Catalytic Oxidation over MnO_x/TiO_2 Catalysts. *J. Phys. Chem. C* **2011**, *115*, 8214–8220. [CrossRef]

Sample Availability: Samples of the compounds are available from the authors.